Heliyon 10 (2024) e37364

Contents lists available at ScienceDirect

Heliyon

journal homepage: www.cell.com/heliyon

Research article

Insulin-like growth factor-2 mRNA-binding protein 2 facilitates post-ischemic angiogenesis by increasing the stability of fibroblast growth factor 2 mRNA and its protein expression

Shuai Ma [a,1], Yiqing Hu [b,1], Wangguo Xu [c,1], Weidong Xiong [a,1], Xinyu Xu [a], Yajie Hou [a], Ying Wang [a], Panke Chen [a], Wenbi Yang [a], Hao Lu [b,**], Yongchao Zhao [a,*]

[a] Department of Cardiology, Affiliated Hospital of Zunyi Medical University, 563000, Zunyi, Guizhou, China
[b] Department of Cardiology, Zhongshan Hospital, Fudan University, Shanghai Institute of Cardiovascular Diseases, 200032, Shanghai, China
[c] Department of Cardiology, Yongchuan Hospital of Chongqing Medical University, 402160, Chongqing, China

ARTICLE INFO

Keywords:
Peripheral arterial disease
Post-ischemic angiogenesis
Insulin-like growth factor-2 mRNA-binding protein 2
Fibroblast growth factor 2
mRNA stability

ABSTRACT

Background: Post-ischemic angiogenesis is crucial for reestablishing blood flow in conditions such as peripheral artery disease (PAD). The role of insulin-like growth factor-2 mRNA-binding protein 2 (IGF2BP2) in post-transcriptional RNA metabolism and its involvement in post-ischemic angiogenesis remains unclear.

Methods: Using a human GEO database and a hind-limb ischemia (HLI) mouse model, the predominant isoform IGF2BP2 in ischemic gastrocnemius tissue was identified. Adeno-associated virus with the *Tie1* promoter induced IGF2BP2 overexpression in the HLI model, evaluating the expression of vascular structural proteins (CD31 and α-SMA) and blood flow recovery after HLI. *In vitro* experiments with human umbilical vein endothelial cells (HUVECs) demonstrated that lentivirus-mediated IGF2BP2 overexpression upregulates cell proliferation, migration, and tube formation. GeneCards, RNAct databases, and subsequent reverse transcription quantitative polymerase chain reaction (RT-qPCR) predicted IGF2BP2 interactions with fibroblast growth factor 2 (FGF2) mRNA, and actinomycin D treatment, binding site predictions and CLIP-seq data further confirmed this interaction. Furthermore, western blotting, enzyme-linked immunosorbent assay, and RNA immunoprecipitation followed by RT-qPCR were performed to validate IGF2BP2's interaction with *FGF2* mRNA and to assess its role in stabilizing *FGF2* mRNA, as well as its impact on FGF2 protein expression.

Results: HLI reduced IGF2BP2 expression in the gastrocnemius tissue, which gradually increased during blood flow recovery. IGF2BP2 overexpression in HLI mice accelerated blood flow recovery and increased capillary and small artery densities. The overexpression of IGF2BP2 in HUVECs stimulated proliferation, migration, and tube formation by interacting with *FGF2* mRNA to

* Corresponding author. Department of Cardiology, Affiliated Hospital of Zunyi Medical University, No. 149 of Road Dalian, District Huichuan, Zunyi, 563000, China.
** Corresponding author. Department of Cardiology, Zhongshan Hospital, Fudan University, Shanghai Institute of Cardiovascular Diseases, No. 1609 of Road Xietu, District Xuhui, Shanghai, 200032, China.
E-mail addresses: lu.hao@zs-hospital.sh.cn (H. Lu), yongchaozhao@zmu.edu.cn (Y. Zhao).
[1] These authors contributed equally.

https://doi.org/10.1016/j.heliyon.2024.e37364
Received 26 May 2024; Received in revised form 1 September 2024; Accepted 2 September 2024
Available online 3 September 2024

increase its stability. This interaction resulted in increased levels of FGF2 protein and secretion, ultimately promoting angiogenesis.
Conclusions: IGF2BP2 contributes to blood flow restoration post-ischemia *in vivo* and promotes angiogenesis in HUVECs by enhancing *FGF2* mRNA stability and FGF2 protein expression and secretion. These findings underscore IGF2BP2's therapeutic potential in ischemic conditions, such as PAD.

1. Introduction

Ischemic cardiovascular diseases include coronary artery, cerebrovascular, and peripheral arterial diseases (PAD). These diseases are a significant burden on healthcare systems worldwide owing to the increasing prevalence of metabolic disorders and the aging population [1–3]. Patients with advanced PAD experience various symptoms, such as claudication, critical limb ischemia, ulcer development, and gangrene [4]. Unfortunately, conventional pharmacological therapies have proven ineffective in certain individuals, leading to the need for endovascular treatment and, in severe cases, amputation of the lower limb [5].

The primary feature of ischemic conditions is vascular occlusion, which is often exacerbated by insufficient angiogenesis [6]. Revascularization remains the standard approach for managing ischemic diseases. Novel therapies aimed at restoring blood flow such as molecular targeting to achieve therapeutic angiogenesis are still under development [7,8]. To develop more efficient pharmacological remedies, the pivotal molecules involved in angiogenesis pathways must first be identified [9].

The insulin-like growth factor-2 mRNA-binding proteins (IGF2BPs) include IGF2BP1, IGF2BP2, and IGF2BP3. IGF2BP is a highly conserved RNA-binding protein family that post-transcriptionally regulates target transcripts. These proteins play critical roles in various cellular processes, physiological functions, and pathological conditions, including cancer development and progression [10]. Among them, IGF2BP2 is the least explored member of this family, although it is known to function as an N6-methyladenosine (m6A) recognition factor [11]. Additionally, IGF2BP2 may influence the stability and translation of target transcripts, thereby affecting diverse physiological and pathological processes, including embryonic development, metabolic diseases and cancer [11–14]. However, the involvement of IGF2BP2 in post-ischemic angiogenesis remains unclear.

Herein, a mouse hind-limb ischemia (HLI) model was established to study the effect of IGF2BP2 on blood flow recovery and post-ischemic angiogenesis. We also evaluated the effect of IGF2BP2 on the proliferation, migration, and tube-forming capacity of human umbilical vein endothelial cells (HUVECs) *in vitro*. To understand the underlying mechanism, we examined the interaction between IGF2BP2 and fibroblast growth factor 2 (*FGF2*) mRNA, a well-known pro-angiogenic factor [12,15,16], along with its effect on the stability of *FGF2* mRNA. Our findings demonstrated that IGF2BP2 promotes blood flow recovery and angiogenesis post-ischemia. IGF2BP2 positively affected the proliferation, migration, and tube-forming capacity of HUVECs. An interaction between IGF2BP2 and *FGF2* mRNA was identified, highlighting its role in modulating FGF2 expression and subsequently promoting angiogenesis in HUVECs. Our study revealed the pivotal function of IGF2BP2 in facilitating blood flow recovery and post-ischemic angiogenesis, thus presenting a potential therapeutic target for ischemic cardiovascular diseases, including PAD.

2. Materials and methods

All experiments involving animals were carried out in full compliance with the regulations specified in the "Guide for the Care and Use of Laboratory Animals," established by the National Academy of Sciences and issued by the National Institutes of Health. The Animal Care and Utilization Committee of Zunyi Medical University approved this study (Appl. No. ZMU21-2207-011). Details regarding the primers, antibodies, and small interfering RNAs (siRNAs) used in this study are listed in Supplementary Materials.

2.1. Cell culture

HUVECs were acquired from Fudan IBS Cell Center (Shanghai, China). They were validated by STR profiling and tested negative for *Mycoplasma*. The cells were grown in DMEM (#1791920, Gibco, Grand Island, NY, USA) supplemented with 10 % FBS (#04-001-1A, BioInd, Kibbutz, Israel) and 1 % penicillin/streptomycin (#10378016, Gibco, Grand Island, NY, USA). They were cultured under standard incubation conditions at 37 °C with a 5 % CO_2 atmosphere.

2.2. Induction of hind-limb ischemia (HLI) and assessment of blood flow recovery

The HLI model was established as previously described [17] using 8-week old male mice from the C57/BL6 strain (GemPharmatech, Nanjing, Jiangsu, China). Femoral artery ligation was performed in the left hind limb of each mouse. Briefly, mice were anesthetized with 1.5–2% isoflurane vaporized in oxygen and were then placed on a heated blanket to maintain their body temperature. The surgical procedure involved making a small incision (~10 mm) in the skin of the hind limb directly over the femoral vasculature. The femoral artery and vein were meticulously isolated from the nerve and ligated (5-0 silk sutures) proximal to the outlet of the profundal femoral artery and distal to the outlet of the saphenous artery. The femoral artery was excised between ligations. For wound closure, a single-layer technique employing 4-0 prolene sutures was used. A laser Doppler ultrasound scanning system (PeriScan PIM 3 system, Perimed, Stockholm, Sweden) was used to evaluate blood flow before and after HLI (on days 0, 3, 7, 14, and 21).

The perfusion ratio in the ischemic hind limb relative to that in the non-ischemic hind limb was determined based on the average flux units measured from the knee to the toe.

2.3. Reverse transcription quantitative polymerase chain reaction (RT-qPCR)

RNA was isolated using TRIzol reagent (#15596026; Invitrogen, Carlsbad, CA, USA) according to the manufacturer's protocol. Subsequently, 1 μg RNA was subjected to reverse transcription using PrimeScript RT kit (#RR036A; TaKaRa, Tokyo, Japan). The resulting cDNA was amplified using the SYBR Green dye (#RR420A; TaKaRa, Tokyo, Japan) on a CFX96 Real-Time PCR Detection System (Bio-Rad Laboratories Inc., Hercules, CA, USA). Each reaction mix had a total volume of 20 μL and consisted of 10 μL SYBR Green, 2 μL template DNA, 1 μL forward primers, 1 μL reverse primers, and 6 μL ddH_2O. The two-step PCR amplification involved the specific parameters of 30 s at 95 °C, followed by 39 cycles of 5 s at 95 °C, and 30 s at 60 °C. For data analysis, gene expression levels were normalized to *Actb* (encoding β-actin) with the standard $2^{-\Delta\Delta Ct}$ quantification method. The detailed primer sequences are listed in Supplementary Table 1.

2.4. Western blotting

Sodium dodecyl sulfate-polyacrylamide gel electrophoresis was used to separate equal amounts of the protein extracts. The proteins were transferred to polyvinylidene difluoride membranes, blocked with 5 % bovine serum albumin (BSA), and then incubated with primary antibodies at 4 °C overnight. After thoroughly rinsing with Tris-buffered saline and Tween, the membranes were incubated with horseradish peroxidase-conjugated secondary antibodies at ambient temperature 22 °C for 60 min. Protein visualization was achieved using the ChemiDoc Imaging System (Bio-Rad, CA, USA). The density of protein bands was determined with NIH ImageJ software (version 1.50i, NIH, Washington, WA, USA, 2016) after normalization to β-actin. The antibodies ustilized in Western blotting analysis are listed in Supplementary Table 2.

2.5. Delivery of Adeno-associated virus (AAV) to mice gastrocnemius

AAV was delivered to the gastrocnemius muscle according to the manufacturer's instructions (Hanbio Biotechnology Co., Ltd., Shanghai, China). Briefly, an AAV containing *Tie1*, a specific endothelial promoter, was generated to facilitate the overexpression of IGF2BP2 with enhanced endothelial targeting. To achieve AAV-mediated *Igf2bp2* gene overexpression, a total of 1×10^{11} viral genomes per milliliter (v.g./mL) of control AAV (*oe-Ctrl*) or overexpression AAV (*oe-Igf2bp2*) were diluted in 10 μL of phosphate-buffered saline (PBS) and injected into the gastrocnemius of wild-type mice 4 weeks before HLI induction. The efficacy of IGF2BP2 overexpression was assessed using RT-qPCR and western blotting analysis prior to the HLI procedure.

2.6. Immunofluorescence analysis of gastrocnemius tissues

Gastrocnemius tissues were fixed in 4 % paraformaldehyde at room temperature and subsequently dehydrated in 30 % sucrose. Optimal cutting temperature compound was used to embed the tissues, and sections were then cut at a thickness of 6–8 μm. Triton X-100 (0.5 %) was added to the sections to promote permeability, followed by blocking with 5 % BSA for 1 h at room temperature. Prediluted antibodies against CD31 and alpha-smooth muscle actin (α-SMA) were then incubated with the sections at 4 °C overnight. Following incubation with the primary antibody, the sections were incubated with fluorescently labeled secondary antibodies for 1 h at room temperature. Cell nuclei were stained with DAPI to aid visualization. Finally, a fluorescence microscope was used to capture images and observe the labeled structures and cellular components within the gastrocnemius tissue. The antibodies used in the immunofluorescence studies are listed in Supplementary Table 2.

2.7. Overexpression of IGF2BP2 in HUVECs

Lentivirus as recommended by the manufacturer (Hanbio Biotechnology Co., Ltd., Shanghai, China) was used to overexpress IGF2BP2 in HUVECs. Briefly, HUVECs were exposed to the control lentivirus (*oe-Ctrl*) or to IGF2BP2 overexpression lentivirus (*oe-IGF2BP2*) for 8 h (multiplicity of infection = 10). Additionally, 10 μg/mL of polybrene (#TR-1003; Sigma, St. Louis, MO, USA) was added to improve the infection efficiency. After 8 h, the lentivirus- and Polybrene-containing media were replaced with fresh complete medium. After 24 h of infection, RT-qPCR and western blotting analyses were conducted to evaluate the efficacy of IGF2BP2 overexpression in HUVECs.

2.8. Transfection with siRNA

HUVECs were seeded in 6-well plates and allowed to grow overnight. Cells were then transfected with *FGF2* siRNA (*siFGF2*) or negative control siRNA (*siCtrl*), acquired from RiboBio Co., Ltd. (Guangzhou, China). Lipofectamine RNAiMAX Transfection Reagent (#13778075; Thermo Fisher Scientific, Waltham, MA, USA) was used for transfection according to the manufacturer's instructions. In brief, 2.5 μL of siRNA and 7.5 μL of transfection reagents were diluted in 250 μL of DMEM. The resulting mixture was then added to 1.725 mL of DMEM containing 10 % FBS, which was subsequently added into each well. The cells were then incubated at 37 °C for 24 h to facilitate transfection. The sequences of the *IGF2BP2* siRNAs used in this experiment are shown in Supplementary Table 3.

2.9. Cell counting Kit-8 (CCK-8) and 5'Ethynyl-2'-Deoxyuridine (EdU) proliferation assays

CCK-8 (#WH1199; Biotechwell, Shanghai, China) and EdU (#C10310-1; RiboBio, Guangzhou, China) assays were performed according to the manufacturer's instructions. IGF2BP2 overexpression and FGF2 knockdown in HUVECs were conducted as follows. Lentiviral transfection (*oe-Ctrl* and *oe-IGF2BP2*) was performed for 24 h, followed by siRNA-mediated suppression (*siCtrl* and *siFGF2*). Following a 24-h recuperation period post-siRNA transfection, HUVECs were dissociated with 0.25 % trypsin and then reseeded at 5000 cells per well in a 96-well plate. Subsequently, the HUVECs were incubated with 10 μL of CCK-8 staining solution per well for an additional 2 h at 37 °C. The optical density (OD) was measured at 450 nm using a microplate reader (Synergy H4; BioTek Instruments, Inc., Winooski, VT, USA). For the EdU assay, following a 24-h recuperation period post-siRNA transfection, HUVECs were cultured with fresh medium containing a 50 μM EdU solution for a 2-h incubation period. The cells were then fixed in 4 % paraformaldehyde, decolorized with 2 mg/mL glycine, permeabilized with 0.5 % TritonX-100 in PBS, and rinsed three times with PBS. Following this, 1 × Apollo Reaction Cocktail (100 μL) was added to the HUVECs for 30 min. DNA content in each well was examined by staining with 100 μL of 1 × Hoechst 33,342 (diluted 1:100) for 30 min, followed by visualization with a fluorescence microscope.

2.10. Enzyme-linked immunosorbent assay (ELISA)

An FGF2 ELISA kit (Abcam, ab246531) was used to quantify the FGF2 released into the HUVEC culture supernatant. Briefly, IGF2BP2 overexpression and FGF2 knockdown in HUVECs were conducted as described above. Lentiviral transfection (*oe-Ctrl* and *oe-IGF2BP2*) was performed for 24 h, followed by siRNA-mediated suppression (*siCtrl* and *siFGF2*). When the knockdown procedure was initiated, the medium was augmented with a protease inhibitor cocktail (Sigma, P1860) at a ratio of 1:600. Following a 24-h recuperation period post-siRNA transfection, the supernatant of the medium was harvested and centrifuged at 1000 rpm for 10 min. Following the guidelines provided by the manufacturer, the ELISA assay was then performed. Using the supplied diluent, samples were diluted 1:20, while the supernatant was diluted 1:10. The FGF2 ELISA units were calculated using the following equation: [(test sample OD value – mean of negative control performed in triplicate OD) × 100/(Mean OD of weak positive control performed in duplicate – mean OD of negative control performed in triplicate)].

2.11. Scratch and transwell assays

The HUVECs were detached using 0.25 % trypsin and seeded into 24-well plates. Once the cells had formed monolayers at approximately 70–80 % confluency, a straight scratch was carefully made across the center of each well using a sterile 10 μL pipette tip. Subsequently, the cells were gently washed twice with medium to remove any detached HUVECs. HUVECs were then cultured for an additional 24 h, during which the scratch widths were visualized under a microscope. The width distances were quantitatively evaluated using Image J software. Furthermore, a migration assay was performed using a 24-well Boyden chamber with porous polycarbonate membrane inserts (8-μm pore size; Costar, Corning, NY, USA). Briefly, 10,000 HUVECs were suspended in 200 μL of DMEM supplemented with 0.1 % FBS and added to the upper chamber, while the lower chamber was filled with 500 μL of DMEM supplemented with 10 % FBS. After incubation for 24 h, the cells that migrated across the filter were washed, stained with 0.1 % crystal violet, fixed with 4 % paraformaldehyde, and photographed under a microscope. The number of migrating cells was determined using NIH Image J software.

2.12. Tube formation assay

After treatment with siRNAs or lentiviral vectors, around 15,000 HUVECs were resuspended in 50 μL of endothelial cell growth medium (#C-22010; PromoCell, Heidelberg, Germany) and seeded onto a 10 μL angiogenesis slide (#81506; Ibidi, Planegg, Germany) that had been pre-coated with polymerization growth factor-reduced Matrigel (#356231; BD Biosciences, Oxford, UK). The cells were then incubated for 3 h to enable tube formation. Following this, the slide was washed meticulously to remove floating cells and 50 μL of calcein (#2049068; Invitrogen, Carlsbad, CA, USA) diluted in a serum-free medium (1:160 dilution) was added. The mixture was incubated in the dark for 30 min at room temperature 22 °C. Excess calcein was removed by washing the slides three times with PBS. Images were captured using a fluorescence microscope. Tube formation was analyzed using the Angiogenesis Analyzer plugin in Image J software, with Tube Length used as the metric for statistical analysis. Following the collection of tube length data, normalization was performed to facilitate comparison between the control and experimental groups. For normalization, the mean tube length for each group (control and experimental) was calculated, and then each group's mean tube length was divided by the mean tube length of the control group. This eliminated differences in measurement units and scales, making it easier to compare the tube formation results between the control and experimental groups.

2.13. RNA immunoprecipitation (RIP) followed by RT-qPCR (RIP-qPCR)

RIP-qPCR was conducted using the a Magna RIP-RNA Binding Protein Immunoprecipitation Kit (Millipore, Bedford, MA, USA) following the manufacturer's guidelines. Initially, 200 μg of total RNA was extracted from HUVECs infected with either the control lentivirus (*oe-Ctrl*) or the overexpression lentivirus (*oe-IGF2BP2*). Chemically fragmented RNA (~200 nucleotides) was then incubated overnight with either mouse anti-IGF2BP2 antibody or mouse IgG-linked beads in 1 × IP buffer at 4 °C. Subsequently, the RNA underwent immunoprecipitation with beads and was eluted by competing with free IGF2BP2. The RNA was then recovered using the

RNeasy kit (Qiagen, Hilden, Germany). The enrichment of *FGF2* mRNA in each sample was assessed via RT-qPCR, and the outcomes were calculated by normalizing to a 10-fold input. The specific antibodies utilized for the RIP-qPCR are listed in Supplementary Table 2, and the primer sequences for *FGF2* mRNA used in the RIP-qPCR analysis are listed in Supplementary Table 4.

2.14. Detection of FGF2 mRNA half-life

HUVECs were plated in 6-well dishes at a density of 2×10^5 cells/well in 2 mL of DMEM. Following infection with either the *oe-Ctrl* or *oe-IGF2BP2* lentivirus, actinomycin D stock (1 mg/mL) was diluted in 100 μL of medium and added dropwise into each well. Samples were collected at 0, 1, 2, 4, 6, and 8 h after the addition of actinomycin D. Cell pellets were collected in 1 mL TRIzol reagent. Total RNA was extracted and reverse transcription was performed for evaluation via RT-qPCR. To calculate mRNA levels, the average Ct value at each time point was normalized to the Ct value at 0 h. To assess the relative degradation rate of mRNA and its half-life, non-linear regression curve fitting with the one-phase decay model was employed (GraphPad Prism 8, San Diego, CA, USA). The mRNA degradation rate (K decay) was estimated using the following equation: ln(C/C0) = –K decay(t), where t indicates the time of transcription inhibition (h), C represents the mRNA quantity at time t, and C0 represent the mRNA quantity at time 0. The mRNA half-life (t1/2) was calculated using the equation: ln(1/2) = K decay (t1/2), where t(1/2) = ln(2)/K decay, which represents the time at which 50 % of the mRNA decayed.

2.15. Statistical analysis

Data are presented as mean ± standard deviation (SD). Two-tailed, unpaired Student's *t*-test was used for group comparisons, unless stated otherwise. Data comparisons involving more than two groups were conducted using the Kruskal–Wallis test for multiple comparisons. All experiments were performed and repeated four to six times to ensure the reliability and consistency of the results. A *p*-value <0.05 was considered statistically significant. Statistical analyses were conducted using the GraphPad Prism 8.0 software (GraphPad Prism Software Inc., San Diego, CA, USA). For each experiment, representative images were selected that closely align with the average data.

3. Results

3.1. IGF2BP2 is downregulated in the ischemic hind limb

IGF2BP2 expression in the gastrocnemius muscle (data extracted from the public database GSE120642 [18]) was analyzed across healthy adults, PAD patients with intermittent claudication, and PAD patients with critical limb ischemia undergoing limb amputation. The analysis revealing the lowest expression in the latter group (Fig. 1A). We established a mouse model of HLI to mimic the

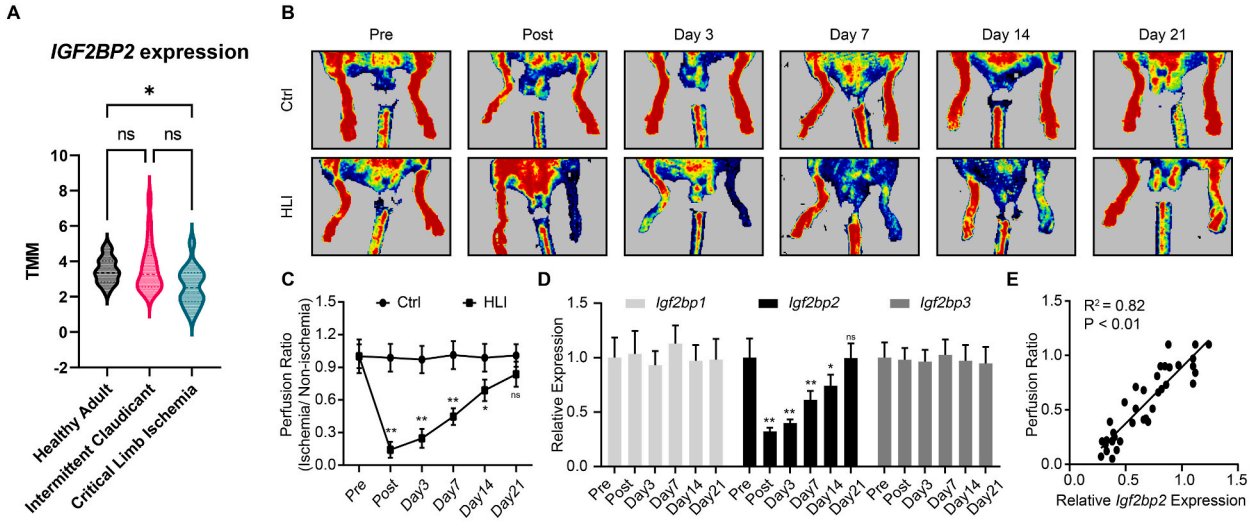

Fig. 1. IGF2BP2 is downregulated in ischemic hind-limb. (A) *IGF2BP2* expression in the gastrocnemius muscle among healthy adults (N = 15), PAD patients with intermittent claudication (N = 20), and PAD patients with critical limb ischemia undergoing limb amputation (N = 16) from the GSE120642 dataset. TMM, Trimmed mean of M values. (B) Representative Laser Doppler imaging showing blood flow recovery in hind-limb ischemia (HLI) mice model. (C) Quantitative analysis of blood flow recovery of left hind limb following mouse HLI induction at indicated time points (N = 6). (D) Quantitative RT-qPCR analysis of gastrocnemius *Igf2bps* expression following HLI at different time points (N = 6). (E) Correlation analysis between *Igf2bp2* expression and blood flow recovery in the left hind limb following HLI induction at indicated time points (N = 6). Data are represented as the mean ± standard deviation (SD). Significance is indicated by $*p < 0.05$, $**p < 0.01$, and "ns" indicates no statistical significance.

pathological processes of clinical PAD. Doppler flow scanning revealed severe ischemic responses in the HLI group following truncation of the femoral artery compared to the sham-operated mice. The most profound ischemia was observed on day 1 after HLI. The blood flow in the ischemic tissue gradually improved over time, peaking on day 21. This confirmed the successful establishment of the mouse HLI model (Fig. 1B and C). *Igf2bp1*, *Igf2bp2*, and *Igf2bp3* expression in ischemic gastrocnemius tissues was assessed using RT-qPCR. Compared with that in the sham-operated group, *Igf2bp1* and *Igf2bp3* expression did not change during the establishment of HLI model, whereas a significant downregulation of *Igf2bp2* expression was observed. Subsequent analyses revealed the progressive upregulation of *Igf2bp2* as blood flow was gradually restored in HLI mice (Fig. 1D). Next, we examined the relationship between the changes in *Igf2bp2* expression and the degree of blood flow recovery after HLI. Higher *Igf2bp2* expression correlated with increased blood flow, suggesting an association between increased *Igf2bp2* mRNA levels and improved post-ischemic angiogenesis (Fig. 1E). These findings indicate a critical role of IGF2BP2 in post-ischemic angiogenesis and warrant further investigation to elucidate the underlying mechanisms.

3.2. IGF2BP2 overexpression facilitates post-ischemic blood flow recovery and angiogenesis

To investigate the role of IGF2BP2 in post-ischemic blood flow recovery and angiogenesis, we used an AAV containing a specific *Tie1* promoter known for its enhanced targeting of endothelial cells. This AAV construct was locally injected into the gastrocnemius muscle tissues of 4-week-old mice to induce high IGF2BP2 expression in the ischemic left hind limb. Four weeks after the injection, RT-qPCR and western blotting analyses were performed to assess the efficiency of IGF2BP2 overexpression. At the 21-day follow-up, Doppler scanning was used to evaluate the restoration of blood flow, while immunofluorescence was employed to assess capillary density (indicated by CD31) and small arteriolar density (indicated by a-SMA) in sections of gastrocnemius tissue from the left hind limb (Fig. 2A). RT-qPCR and western blotting results showed significant upregulation of IGF2BP2 at both the gene and protein level in the *oe-Igf2bp2* group (Fig. 2B–D). Moreover, Doppler scanning revealed that IGF2BP2 overexpression significantly promoted blood flow recovery after HLI compared to that in the control group (Fig. 2E and F). Additionally, immunofluorescence analysis showed that the IGF2BP2 overexpression group exhibited increased CD31-positive and a-SMA-positive signals. This indicates a significant correlation between IGF2BP2 overexpression and enhanced capillary density and small arterial density (Fig. 2G and H).

3.3. IGF2BP2 overexpression promotes angiogenesis in HUVECs

To investigate the role of IGF2BP2 in angiogenesis *in vitro*, HUVECs were cultured and lentiviral vectors were subsequently employed to induce high expression of IGF2BP2. The efficiency of IGF2BP2 overexpression after lentiviral infection was confirmed with RT-qPCR and western blotting analyses. These results revealed a significant increase in IGF2BP2 expression compared to that in the empty vector viral infection group (Fig. 3A–C). The effects of IGF2BP2 overexpression on the proliferation, migration, and tube-forming phenotype of HUVECs were examined. IGF2BP2 overexpression resulted in greater cell viability (Fig. 3D), increased numbers of EdU-positive cells (Fig. 3E), reduced scratch areas (Fig. 3F), elevated numbers of migrating cells (Fig. 3G), and enhanced tube-formation (Fig. 3H) compared to those in control group. Collectively, these findings demonstrated that IGF2BP2 overexpression promotes angiogenesis in HUVECs *in vitro*.

3.4. IGF2BP2 binds to FGF2 mRNA and inhibits its degradation

We investigated the molecular mechanisms by which IGF2BP2 promotes angiogenesis in HUVECs. Initially, bioinformatics analysis was conducted by searching the GeneCards database (https://www.genecards.org/) for the top 100 genes associated with angiogenesis. Simultaneously, the RNAct database (http://rnact.crg.eu/) was used to screen for mRNAs that could potentially bind to the IGF2BP2 protein, leading to the identification of 125 candidate targets. By integrating candidate genes obtained from the two databases, we identified three potential targets. These included the Wnt family member 1 (*WNT1*), mitogen-activated protein kinase 3 (*MAPK3*), and fibroblast growth factor 2 (*FGF2*) (Fig. 4A). IGF2BP2 serves as an m6A recognition protein that binds to and inhibits the degradation of m6A-modified mRNAs. Therefore, it functions as a post-transcriptional mechanism to increase the mRNA expression. Of the three potential mRNA targets, significant upregulation was observed only for *FGF2* mRNA (Fig. 4B). To explore this mechanism in more depth, actinomycin D and RT-qPCR were employed to demonstrate that IGF2BP2 overexpression significantly inhibited the degradation of *FGF2* mRNA, thereby prolonging its half-life (Fig. 4C). Actinomycin D is a transcriptional inhibitor that was used in this study to block new RNA synthesis, allowing for the measurement of mRNA decay rates. These results suggest that IGF2BP2 stabilizes *FGF2* mRNA by binding to it, thereby preventing its degradation. Furthermore, to test whether the IGF2BP2 protein could bind to the *FGF2* mRNA transcript, we utilized established online databases that catalog RNA-binding protein (RBP) interaction sites on transcripts. Subsequently, we corroborated these findings by analyzing relevant sequencing datasets to validate the potential binding interactions. For both human and mouse species, results from DeepBind [19], FIMO (https://meme-suite.org/meme/doc/fimo.html?man_type=web), and TESS, as presented in the RBP Binding Sites Modual in POSTAR3 (http://111.198.139.65/RBS.html), consistently reveal multiple binding sites for IGF2BP2 on the *FGF2* mRNA transcript. We identified the top 10 predicted binding sites (or all sites, if fewer than 10 were available), sorted by score. These predictions strongly suggested that IGF2BP2 has the potential to bind to the *FGF2* mRNA transcript at multiple loci (Supplementary Table 5). Additionally, we predicted the binding potentials between IGF2BP2 and *FGF2* mRNA transcript using RPISeq (http://pridb.gdcb.iastate.edu/RPISeq/). Sequence-based interaction predictions yielded interaction probabilities of 0.7 with the RF classifier and 0.93 with the SVM classifier. According to the official explanation provided by RPISeq, predictions with probabilities greater than 0.5 are considered positive. Therefore, it is highly likely that IGF2BP2

and *FGF2* mRNA transcripts interact with each other. Finally, to validate these prediction results, we sought sequencing data that could corroborate the binding interactions. Analysis of CLIP-seq data (GSE192792 [20]) confirmed the presence of three binding sites on the *FGF2* mRNA transcript sourced from humans. Raw sequence data were downloaded from the GEO database and mapped onto the

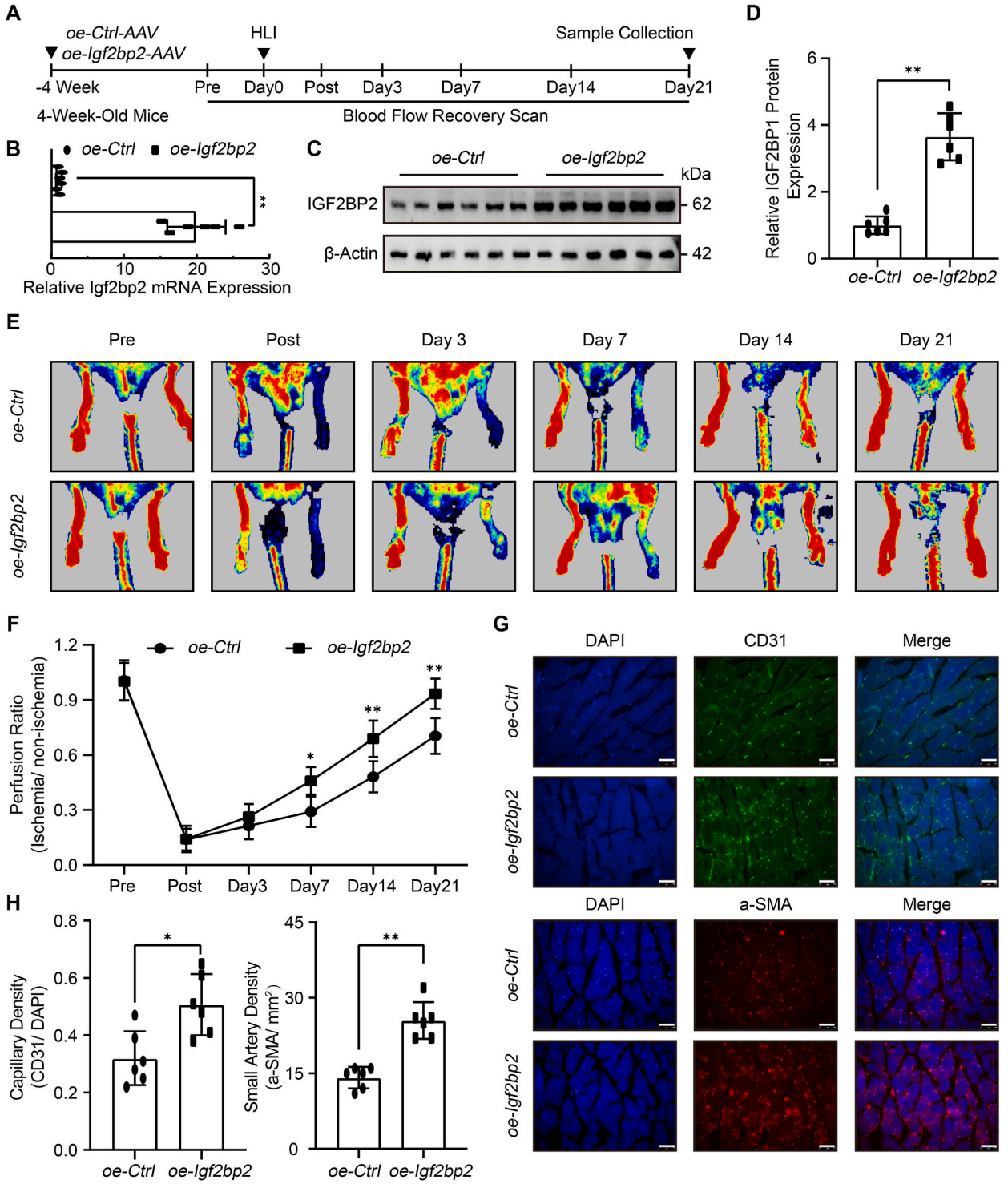

(caption on next page)

Fig. 2. IGF2BP2 overexpression facilitates post-ischemic blood flow recovery and angiogenesis. (A) Schematic representation of *in vivo* injection of IGF2BP2-overexpressing AAV (*oe-Igf2bp2*) or control AAV (*oe-Ctrl*) into the gastrocnemius muscle of mice before hind-limb ischemia (HLI) induction. Laser Doppler imaging was performed to monitor blood flow recovery at specific time points, and samples were collected on day 21 for further analysis. (B) Quantification of RT-qPCR data depicting the mRNA expression level of *Igf2bp2* (N = 6). (C,D) Representative images of western blotting and quantification of IGF2BP2 protein expression (N = 6). (E) Representative Laser Doppler images showing blood flow scans. (F) Quantitative analysis of blood flow recovery (N = 6). (G) Representative images of gastrocnemius immunofluorescence staining, displaying relative CD31 (upper panel) and α-SMA (lower panel) expression. Scale bar = 100 μm. (H) Quantitative assessment of capillary density (CD31/DAPI) and small artery density (α-SMA/mm^2) (N = 6). Data are represented as the mean ± standard deviation (SD). Significance is indicated by $^*p < 0.05$, and $^{**}p < 0.01$.

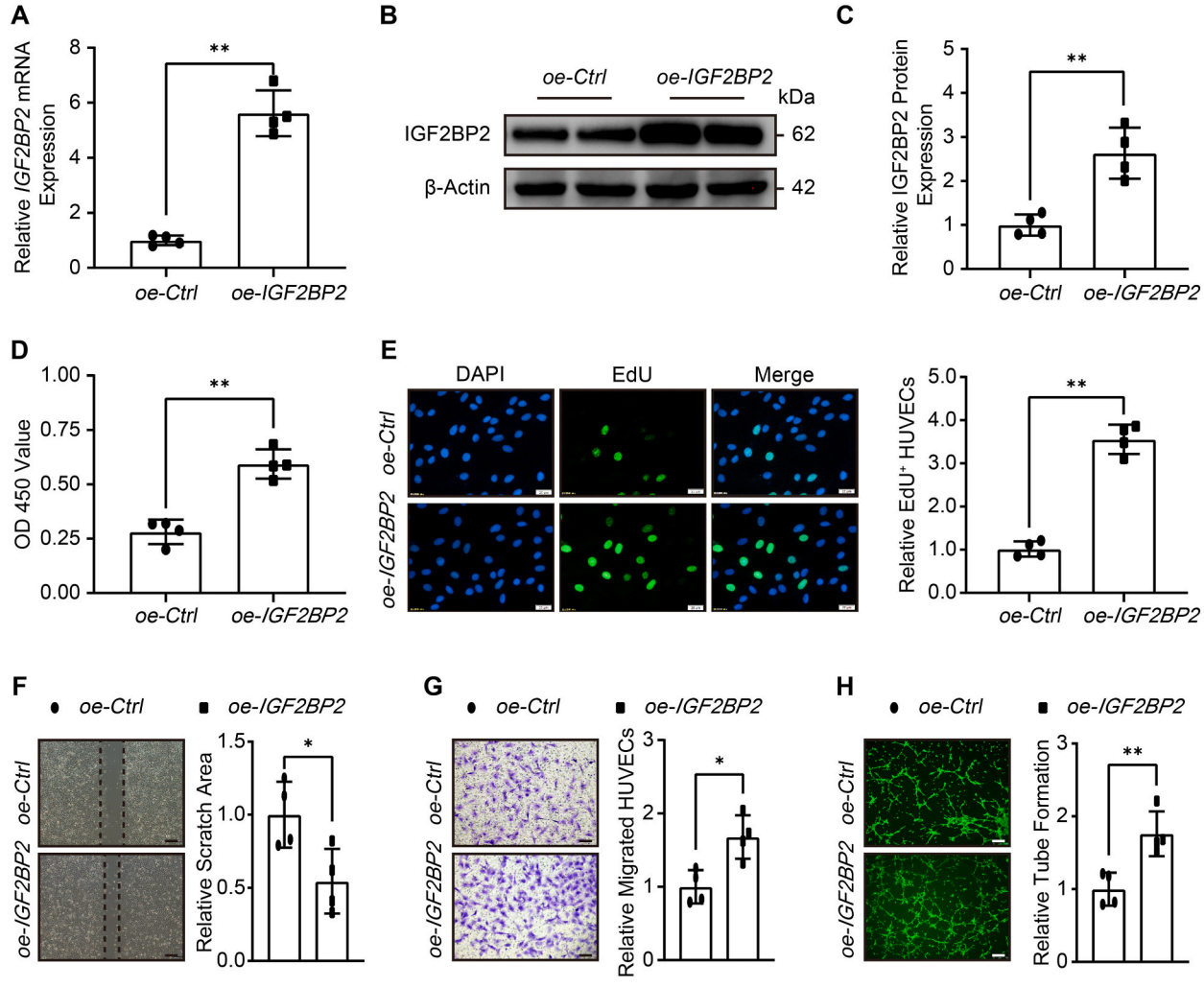

Fig. 3. IGF2BP2 overexpression promotes angiogenesis in HUVECs. (A) Quantitative RT-qPCR analysis depicting *IGF2BP2* expression following lentivirus infection (N = 4). (B,C) Representative images of western blotting and quantification (N = 4) of IGF2BP2 protein expression. (D) Quantification of CCK-8 showing HUVECs viability (N = 4). (E) Representative imagesof EdU staining (left panel) and quantification (right panel) of EdU-positive HUVECs, indicating active cell proliferation. Scale bar = 20 μm. OD, optical density. (F) Representative scratch assay images (left panel) and quantification (right panel) (N = 4) of scratch area, indicating cell migration. Scale bar = 100 μm. (G) Representative Transwell assay images (left panel) and quantification (right panel) (N = 4) of number of migrated HUVECs, indicating cell migration. Scale bar = 200 μm. (H) Representative tube formation assay images (left panel) and quantification (right panel) (N = 4) of tube-like structures formed by HUVECs, indicating angiogenesis. Scale bar = 500 μm. All images were obtained from four random microscopic fields for each group and subsequently analyzed using NIH ImageJ software. Data are represented as the mean ± standard deviation (SD). Significance is indicated by $^*p < 0.05$, and $^{**}p < 0.01$.

reference genome. Visualizations generated by the Integrative Genomics Viewer revealed a pronounced peak at the 5′ end of the sequencing data, suggesting a potential binding site (Fig. 4D). This empirical evidence supports the predicted interactions between IGF2BP2 and *FGF2* mRNA. Consequently, this stabilization could lead to an increase in FGF2 protein translation and, ultimately, to the

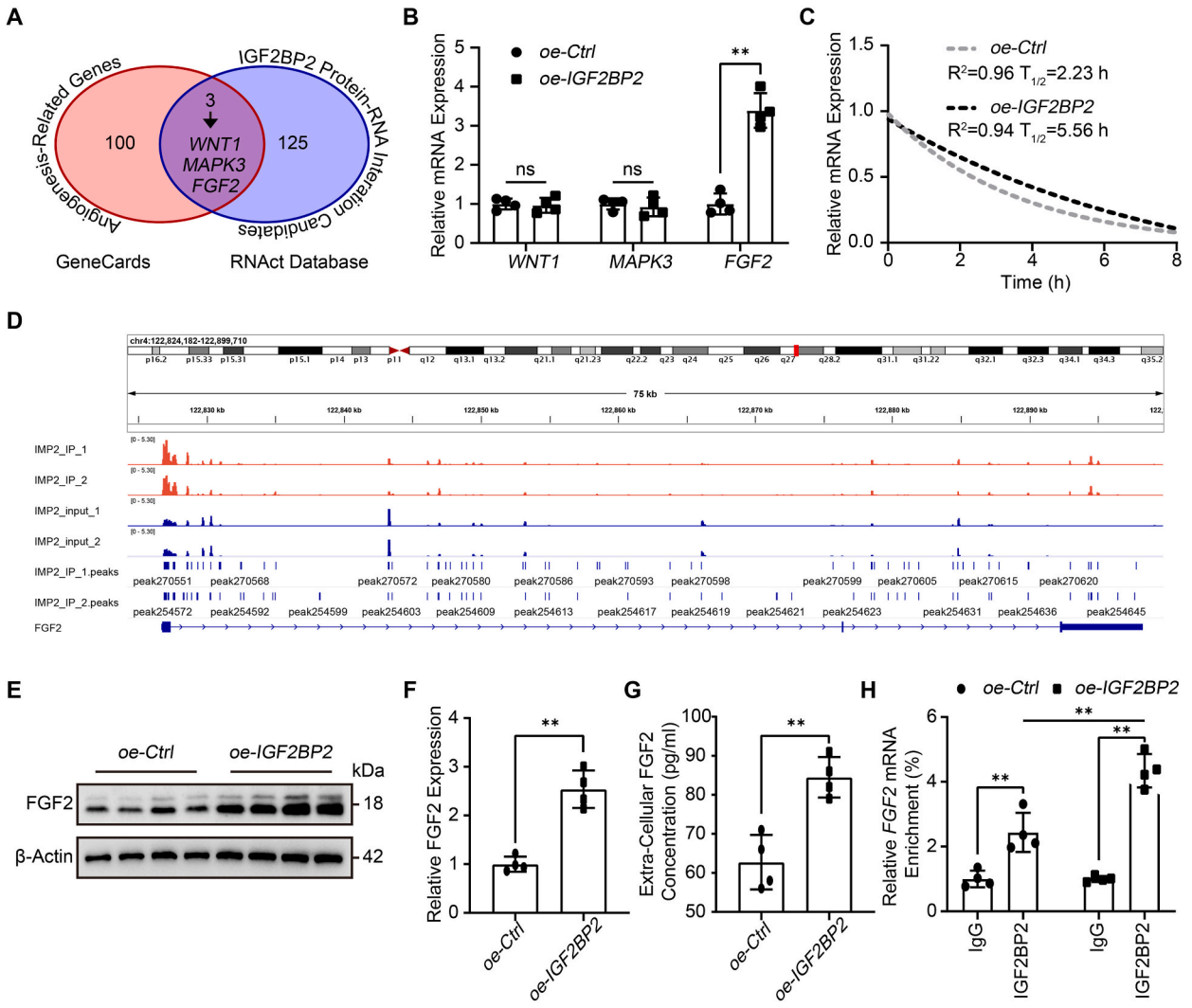

Fig. 4. IGF2BP2 binds to *FGF2* mRNA and inhibits its degradation. (A) Venn diagram displaying the intersection between the top 100 angiogenesis-related genes from the GeneCards database and the IGF2BP2 protein-RNA interaction candidates predicted from the RNAct database. (B) Quantitative analysis of RT-qPCR validation for candidate mRNA expression (N = 4). (C) Quantitative analysis of RT-qPCR data revealing the half-life of *FGF2* mRNA by tracking transcript abundance at various time points following transcriptional inhibition with actinomycin D (N = 4). (D) Visualization of IGF2BP2 binding sites on *FGF2* mRNA transcript using CLIP-seq data. (E,F) Representative images of western blotting and quantification (N = 4) of FGF2 protein expression. (G) Quantification of extracellular FGF2 protein expression via ELISA assay (N = 4). (H) Quantification of RIP-qPCR analysis illustrating the immunoprecipitation of *FGF2* mRNA upon incubation with either anti-IgG or anti-IGF2BP2 beads (N = 4). All data presented are expressed as the mean ± standard deviation (SD). Statistical significance is indicated by $^{**}p < 0.01$, while "ns" denotes no statistical significance.

upregulation of FGF2 protein levels. Western blotting analysis confirmed increased protein expression of FGF2 in the IGF2BP2 overexpression group (Fig. 4E and F). Because FGF2 is a secreted protein, we assessed its content in the extracellular medium using ELISA. This revealed a marked upregulation of FGF2 secretion into the extracellular medium in the IGF2BP2 overexpression group compared to that in the control group (Fig. 4G). Finally, RIP-qPCR was performed to validate the binding of IGF2BP2 to *FGF2* mRNA. This confirmed that the IGF2BP2 protein effectively bound to *FGF2* mRNA, resulting in a significant upregulation of bound *FGF2* mRNA following IGF2BP2 overexpression (Fig. 4H). Collectively, these findings highlight the potential role of IGF2BP2 in regulating the stability and translation of *FGF2* mRNA, thereby contributing to the observed increase in FGF2 protein expression.

3.5. *IGF2BP2 promotes angiogenesis in HUVECs via FGF2*

IGF2BP2 has been identified as a key regulator of *FGF2* mRNA expression, contributing to its post-transcriptional stability. However, the precise mechanism through which IGF2BP2 promotes angiogenesis in HUVECs via FGF2 remains elusive. To investigate

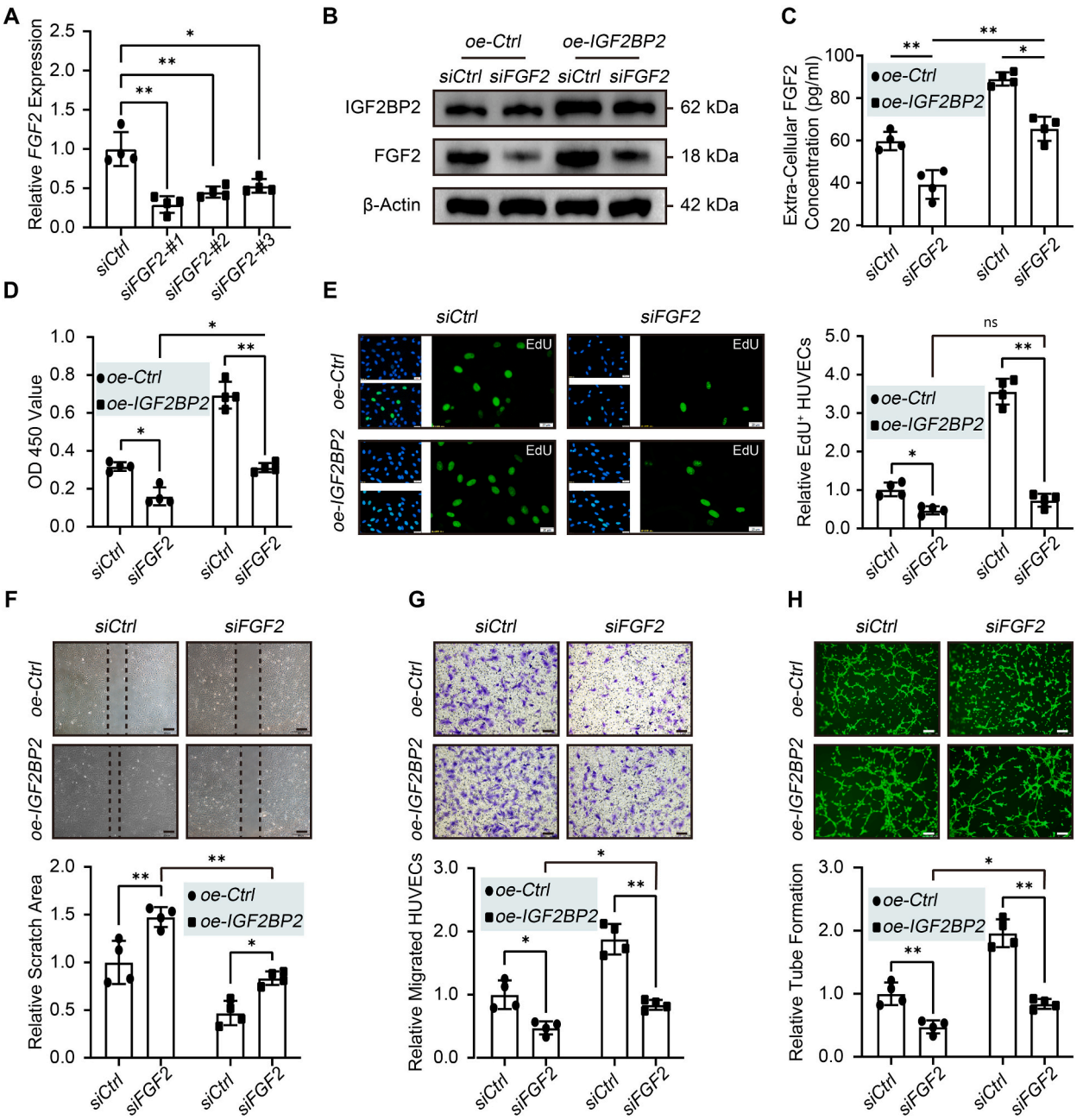

Fig. 5. IGF2BP2 promotes angiogenesis in HUVECs via FGF2. (A) RT-qPCR analysis validating the knock-down efficiency of three pairs of siRNAs targeting *FGF2* mRNA (N = 4). (B) Representative images of western blotting showing the expression levels of IGF2BP2 and FGF2 proteins. (C) Quantification of extracellular FGF2 protein expression with ELISA assay (N = 4). (D) Quantification of CCK-8 assay indicating HUVECs viability (N = 4). OD, optical density. (E) Representative images of EdU staining (left panel) and quantification (right panel) (N = 4) of EdU-positive HUVECs, reflecting active cell proliferation. Scale bar = 20 μm. (F) Representative scratch assay images (upper panel) and quantification (lower panel) (N = 4) of the scratch area, indicating cell migration. Scale bar = 100 μm. (G) Representative Transwell assay images (upper panel) and quantification (lower panel) (N = 4) of the number of migrated HUVECs, reflecting cell migration. Scale bar = 200 μm. (H) Representative tube formation assay images (upper panel) and quantification (lower panel) (N = 4) of tube-like structures formed by HUVECs, indicating angiogenesis. Scale bar = 500 μm. All images were obtained from four random microscopic fields for each group and subsequently analyzed using NIH ImageJ software. Data presented are expressed as the mean ± standard deviation (SD). Statistical significance is indicated by $^{*}p < 0.05$, and $^{**}p < 0.01$.

this, siRNAs targeting *FGF2* mRNA were used to downregulate FGF2 expression. RT-qPCR analysis revealed that all three siRNA pairs significantly reduced *FGF2* expression. *siFGF2-#1* exhibited the best knockdown efficiency (Fig. 5A) and was therefore selected for subsequent experiments. Western blotting and ELISA demonstrated a substantial reduction in FGF2 protein expression in HUVECs and secreted FGF2 protein in the medium, respectively, following *siFGF2-#1* transfection. This was observed in both the control lentivirus-infected and IGF2BP2 overexpressing lentivirus-infected groups (Fig. 5B and C). Nonetheless, IGF2BP2 protein overexpression was able to partially restore FGF2 protein expression and secretion even under FGF2 knockdown conditions (Fig. 5B and C). Further evaluation of the angiogenic phenotype of HUVECs revealed that FGF2 knockdown reduced cell viability (Fig. 5D), decreased the number of EdU-positive cells (Fig. 5E), increased the cell scratch area (Fig. 5F), reduced cell migration (Fig. 5G), and inhibited the tube-forming capacity (Fig. 5H). Collectively, these observations demonstrate that the pro-angiogenic effect of IGF2BP2 overexpression in HUVECs occurs via FGF2.

4. Discussion

This is the first study to reveal a potential role of IGF2BP2 in post-ischemic blood flow recovery and angiogenesis, as well as its associated mechanism. We found that upregulation of IGF2BP2 in mice with HLI was strongly associated with enhanced post-ischemic blood flow recovery and increased capillary and small artery densities. Moreover, *in vitro* experiments with HUVECs demonstrated that overexpression of IGF2BP2 promoted endothelial cell proliferation, migration, and tube formation. The mechanism underlying IGF2BP2 promotion of angiogenesis appears to involve the upregulation of *FGF2* mRNA stability and the subsequent expression and secretion of FGF2 protein (Fig. 6). These findings suggest potential targets for the pharmacological treatment of ischemic diseases.

Atherosclerosis serves as a significant pathological basis for panvascular diseases, with PAD being a vital component of these disorders [21–23]. Current clinical guidelines advocate for several treatments for patients with PAD, all of which aim to control atherosclerosis-related risk factors. These include antiplatelet treatments, statins, angiotensin-converting enzyme inhibitors, and angiotensin receptor blockers [24,25]. Although these interventions lead to some improvement in patient outcomes, revascularization or unavoidable amputation remain the only viable options once symptoms such as intermittent claudication or severe lower-limb ischemia occur [26,27]. Therapeutic angiogenesis involves the induction of growth and proliferation of blood vessels from the existing vasculature. This approach has been investigated in patients with symptomatic PAD over the last two decades. Despite promising preclinical studies on vascular endothelial growth factor (VEGF) and hepatocyte growth factor, large-scale clinical trials have yielded disappointing results [8]. Hence, there is an urgent need for innovative drug development strategies that focus on promoting angiogenesis and restoring blood flow to treat ischemic diseases [28].

The IGF2BP family comprises RNA-binding proteins that play crucial roles in the post-transcriptional regulation of target transcripts. These proteins are involved in various cellular functions and pathologies, including cancer development and progression [10,29]. The IGF2BP family consists of three members (IGF2BP1, IGF2BP2, and IGF2BP3) involved in post-transcriptional mRNA metabolism. Their functions include mRNA transport, translation, and stability regulation of N6-methyladenosine (m6A)-modified mRNA

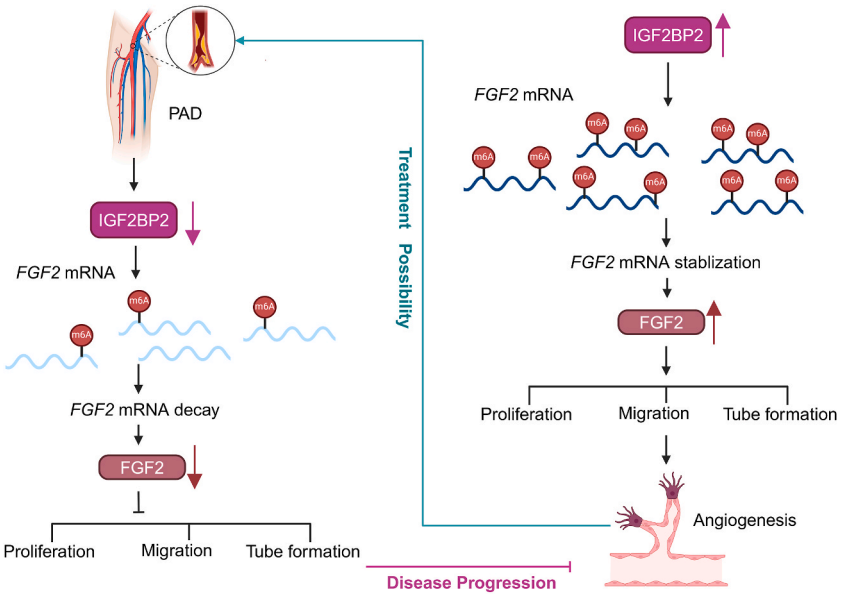

Fig. 6. IGF2BP2 promotes angiogenesis via *FGF2* mRNA stabilization. The left side illustrates how inhibiting IGF2BP2 leads to *FGF2* mRNA decay, reducing FGF2 protein levels and subsequently impairing cell proliferation, migration, and tube formation, which contributes to peripheral artery disease. Conversely, the right side shows that increasing IGF2BP2 stabilizes *FGF2* mRNA, thereby upregulating FGF2 protein levels and enhancing proliferation, migration, tube formation, and ultimately angiogenesis, suggesting a potential treatment approach. This figure was created with BioRender.com.

[30,31]. Dysregulation of IGF2BPs is linked to insulin resistance, diabetes, cancer metastasis, and the expression of oncogenic factors [32–34]. IGF2BP1 controls the alternative splicing of VEGFR1 in endothelial cells, thus making it a potential target for therapeutic angiogenesis intervention [35]. Additionally, IGF2BP3 knockdown in stomach cancer is associated with reduced hypoxia-induced angiogenesis [36]. In colon cancer, IGF2BP3 regulates angiogenesis by binding to *VEGF* mRNA, modulating its expression and stability [37]. Furthermore, some IGF2BP2-mediated tumor angiogenesis mechanisms have been reported in recent studies. A distinct group of lung adenocarcinoma (LUAD) cells expressing IGF2BP2 is an important drivers of angiogenesis and metastasis [38]. The proposed mechanism is that LUAD cell-derived exosomes transfer IGF2BP2 to endothelial cells present in the local microenvironment, thereby stabilizing FLT4 and activating the PI3K-Akt signaling pathway for angiogenesis [38]. The m^6A-mediated HNF1A-AS1/IGF2BP2/CCND1 pathway stabilizes *CCND1* mRNA, thereby promoting cell cycle progression and tumor angiogenesis in colorectal cancer [39]. Moreover, knockdown or knockout of IGF2BP2 could potentially inhibit cancer cell growth and regulate the tumor microenvironment [40]. IGF2BP knockdown in an m^6A-dependent manner suppresses *MYC* mRNA stability and translation in HeLa cells and hepatocellular carcinoma cells [41]. Based on these findings, we hypothesized that IGF2BP2 plays a crucial regulatory role in angiogenesis. Herein, IGF2BP1 and IGF2BP3 expression remained unchanged following the induction of HLI in mice through femoral artery ligation, but IGF2BP2 expression was significantly decreased. The progressive increase in IGF2BP2 expression post-ischemia was significantly and positively correlated with the degree of blood flow recovery. These observations highlight the distinct expression and regulatory patterns of IGF2BP family members in various disease states. In addition, they emphasize the potential value of targeting IGF2BP2 up-regulation in ischemic diseases, particularly in PAD, for future therapeutic applications.

FGF2 has been extensively studied because of its crucial role in angiogenesis through the promotion of endothelial cell proliferation, survival, and sprouting, thereby contributing to both normal and pathological angiogenesis [35]. Although FGF2 is not the sole angiogenic growth factor, it has therapeutic potential for various diseases and conditions such as age-related macular degeneration, achondroplasia, lung cancer, and cancer pain [42]. In the present study, we screened IGF2BP2 candidate targets by combining the GeneCards and RANct databases to identify angiogenesis-related genes and IGF2BP2 protein-RNA interaction candidates. Among the three candidate targets identified, FGF2 emerged as the most promising, mainly because it was significantly upregulated in HUVECs that overexpress IGF2BP2. Furthermore, the half-life of *FGF2* mRNA was significantly prolonged by IGF2BP2, resulting in both intracellular and extracellular increases in FGF2 protein levels. Direct binding of IGF2BP2 to *FGF2* mRNA was confirmed using RIP-qPCR. Importantly, the downregulation of FGF2 reversed angiogenesis in HUVECs, thus providing compelling evidence for the mechanism by which IGF2BP2 regulates angiogenesis in these cells.

Furthermore, the effective concentration of FGF2 for HUVECs is widely utilized in current tissue engineering studies. The efficacy of FGF2 is closely related to its isolation and purification methods. Commercial FGF2 (produced in *E. coli*, GenScript, Cat. No. Z03116-1) and its recombinant version (derived from *P. pastoris* KM71H by Antonín Sedlář et al.) can enhance HUVEC proliferation in a dose-dependent manner, ranging from 5 ng/mL to 250 ng/mL [43]. This finding aligns with FGF2 being a key ingredient in multiple growth media for endothelial cells, and it appears to stimulate HUVEC proliferation more effectively than VEGF-A_{165} [43,44]. Moreover, in biomaterials science and tissue engineering, growth factors are frequently attached to various biomaterials to enhance their bioactivity and mimic extracellular matrix-bound growth factors. The proliferation of HUVECs in 96-well plates pre-coated with recombinant FGF2 at concentrations ranging from 0.01 μM to 10 μM (approximately 0.172–172 μg/mL) was comparable to the growth observed when the growth factors were diluted in the culture media [43]. On day 7 after seeding, HUVECs exhibited the high cell numbers and metabolic activity at 1–10 μM. This increase was more pronounced in wells pre-adsorbed with recombinant FGF2 (compared to VEGF-A_{165}), particularly in terms of cell number [43]. Moreover, FGF2 promotes the growth of both endothelial and stem cells. These cells can differentiate into various types used in cardiovascular tissue engineering, such as vascular smooth muscle cells and endothelial cells [45]. Moreover, the immobilization of VEGF-A_{165} and FGF2 onto surfaces of diverse synthetic and natural biomaterials boosts cell adhesion and proliferation, particularly for endothelial cells, and enhances material biocompatibility [46–49]. For example, FGF-2 and VEGF-A_{165} were recently used to functionalize a fibrin/heparin coating on the interior surface of an ePTFE vascular graft to facilitate endothelialization [50]. However, the specific application mode of the IGF2BP2-FGF2 axis in PAD therapy remains unknown.

Our study had certain limitations. Using flow cytometry for cell sorting or immunofluorescence colocalization based on endothelial cell markers (CD31 or VE-cadherin) and IGF2BP2 for gastrocnemius tissue can provide further validation of the effects of injecting IGF2BP2-overexpressing AAV virus into the gastrocnemius muscle of mice. However, as outlined in our methodology, the AAV vector was constructed using the a *Tie1* promoter, which specifically targets endothelial cells. We used an endothelial-selective *Tie1* promoter to induce IGF2BP2 expression *in vivo* and observed the pro-angiogenic effect of IGF2BP2 overexpression in HUVECs *in vitro*. Furthermore, western blotting and RT-qPCR analyses confirmed successful overexpression of IGF2BP2. Subsequent experiments were primarily conducted using HUVECs. We believe that these approaches are sufficient for substantiating our conclusions. However, further studies are required to confirm the feasibility of IGF2BP2 as a potential therapeutic target.

5. Conclusions

Our findings demonstrate that IGF2BP2 promotes blood flow recovery and angiogenesis post-ischemia. Additionally, IGF2BP2 plays a crucial role in inhibiting the degradation of *FGF2* mRNA, thereby extending its half-life through direct binding. This mechanism ultimately promotes the protein expression and extracellular secretion of FGF2, thereby contributing to enhanced angiogenesis in HUVECs. These findings significantly advance our understanding of the intricate molecular mechanisms underlying angiogenesis. Furthermore, our findings suggest potential therapeutic strategies for targeting these pathways in ischemic-related disorders.

Ethics statement

All experiments involving animals were carried out in full compliance with the regulations specified in the 'Guide for the Care and Use of Laboratory Animals', as established by the National Academy of Sciences and issued by the National Institutes of Health. Furthermore, the experimental protocol received approval from the Animal Care and Utilization Committee of Zunyi Medical University (Appl. No. ZMU21-2207-011, approval on 07/04/2022).

Data availability statement

Data is not available to access in a data repository; however, data included in article/supp. material/referenced in article.

CRediT authorship contribution statement

Shuai Ma: Writing – review & editing, Writing – original draft, Methodology, Formal analysis, Data curation. **Yiqing Hu:** Writing – review & editing, Writing – original draft, Visualization, Validation, Software, Methodology, Formal analysis. **Wangguo Xu:** Writing – original draft, Validation, Supervision, Project administration, Investigation, Conceptualization. **Weidong Xiong:** Writing – original draft, Supervision, Software, Resources, Methodology, Formal analysis, Data curation. **Xinyu Xu:** Validation, Resources, Data curation. **Yajie Hou:** Visualization, Software, Methodology. **Ying Wang:** Visualization, Validation, Supervision, Software. **Panke Chen:** Methodology, Investigation, Formal analysis, Data curation. **Wenbi Yang:** Methodology, Investigation, Formal analysis, Data curation. **Hao Lu:** Writing – review & editing, Visualization, Validation, Supervision, Software, Resources, Project administration, Methodology, Investigation, Funding acquisition, Formal analysis, Data curation, Conceptualization. **Yongchao Zhao:** Writing – review & editing, Writing – original draft, Visualization, Validation, Supervision, Software, Resources, Project administration, Methodology, Investigation, Funding acquisition, Formal analysis, Data curation, Conceptualization.

Declaration of competing interest

The authors declare that they have no known competing financial interests or personal relationships that could have appeared to influence the work reported in this paper.

Acknowledgment

The funding for this study was provided by various organizations including National Natural Science Foundation of China, China (No.: 82470405, 82200290), the Guizhou Provincial Basic Research Program (Natural Science), China (Qiankehe Foundation-ZK [2024] Key 068, Qiankehe Foundation-ZK [2023] General 563, Qiankehe Foundation-ZK [2022] General 671), the Excellent Young Talent Cultivation Project of Zunyi City, China (Zunshi Kehe HZ (2022) 366), and the "Fuqing Scholar" Student Scientific Research Program of Shanghai Medical College, Fudan University, China (No.: FQXZ202301A). We would like to thank Dr. Lin Zeng (NewCore Biotech, Shanghai, 200032, China) for his valuable assistance with the bioinformatics analysis of protein-RNA interaction.

Appendix A. Supplementary data

Supplementary data to this article can be found online at https://doi.org/10.1016/j.heliyon.2024.e37364.

References

[1] B. Zierfuss, M. Catalano, G.-H. Schernthaner, Finally, the big picture of morbidity and mortality in peripheral arterial disease? Atherosclerosis 293 (2020) 92–93, https://doi.org/10.1016/j.atherosclerosis.2019.11.006.
[2] I.J. Kullo, T.W. Rooke, Peripheral artery disease, N. Engl. J. Med. 374 (2016) 861–871, https://doi.org/10.1056/NEJMcp1507631.
[3] B. Balkau, M. Vray, E. Eschwege, Epidemiology of peripheral arterial disease, J. Cardiovasc. Pharmacol. 23 (Suppl 3) (1994) S8–S16.
[4] O. Afify, S. Alkhouri, N. Lauder, Improving symptoms of peripheral artery disease with hirudotherapy, Cureus 13 (2021) e16270, https://doi.org/10.7759/cureus.16270.
[5] A. Lazar, N. Morrissey, Recent advances in endovascular treatment of peripheral arterial disease, F1000Research 9 (2020) 122, https://doi.org/10.12688/f1000research.20398.1.
[6] C. Inampudi, E. Akintoye, T. Ando, A. Briasoulis, Angiogenesis in peripheral arterial disease, Curr. Opin. Pharmacol. 39 (2018) 60–67, https://doi.org/10.1016/j.coph.2018.02.011.
[7] F. Sanada, Y. Taniyama, J. Muratsu, R. Otsu, H. Shimizu, H. Rakugi, R. Morishita, Gene-therapeutic strategies targeting angiogenesis in peripheral artery disease, Medicines 5 (2018) 31, https://doi.org/10.3390/medicines5020031.
[8] S.R. Iyer, B.H. Annex, Therapeutic angiogenesis for peripheral artery disease, JACC Basic Transl. Sci. 2 (2017) 503–512, https://doi.org/10.1016/j.jacbts.2017.07.012.
[9] D.A. Duprez, Pharmacological interventions for peripheral artery disease, Expert Opin. Pharmacother. 8 (2007) 1465–1477, https://doi.org/10.1517/14656566.8.10.1465.
[10] S.M. Korn, C.J. Ulshöfer, T. Schneider, A. Schlundt, Structures and target RNA preferences of the RNA-binding protein family of IGF2BPs: an overview, Structure 29 (2021) 787–803, https://doi.org/10.1016/j.str.2021.05.001.

[11] J. Wang, L. Chen, P. Qiang, The role of IGF2BP2, an m6A reader gene, in human metabolic diseases and cancers, Cancer Cell Int. 21 (2021) 99, https://doi.org/10.1186/s12935-021-01799-x.

[12] S. Mori, N. Hatori, N. Kawaguchi, Y. Hamada, T.-C. Shih, C.-Y. Wu, K.S. Lam, N. Matsuura, H. Yamamoto, Y.K. Takada, Y. Takada, The integrin-binding defective FGF2 mutants potently suppress FGF2 signalling and angiogenesis, Biosci. Rep. 37 (2017), https://doi.org/10.1042/BSR20170173. BSR20170173.

[13] N. Dai, L. Zhao, D. Wrighting, D. Krämer, A. Majithia, Y. Wang, V. Cracan, D. Borges-Rivera, V.K. Mootha, M. Nahrendorf, D.R. Thorburn, L. Minichiello, D. Altshuler, J. Avruch, IGF2BP2/IMP2-Deficient mice resist obesity through enhanced translation of Ucp1 mRNA and other mRNAs encoding mitochondrial proteins, Cell Metab. 21 (2015) 609–621, https://doi.org/10.1016/j.cmet.2015.03.006.

[14] Q. Yang, Y. Ma, Y. Liu, X. Shao, W. Jia, X. Yu, Y. Li, L. Yang, W. Gu, H. Wang, J. Wang, Y. Wang, MNSFβ regulates placental development by conjugating IGF2BP2 to enhance trophoblast cell invasiveness, Cell Prolif. 54 (2021) e13145, https://doi.org/10.1111/cpr.13145.

[15] E. Tassi, A. Al-Attar, A. Aigner, M.R. Swift, K. McDonnell, A. Karavanov, A. Wellstein, Enhancement of fibroblast growth factor (FGF) activity by an FGF-binding protein, J. Biol. Chem. 276 (2001) 40247–40253, https://doi.org/10.1074/jbc.M104933200.

[16] C. Butt, S. Lim, C. Greenwood, P. Rahman, VEGF, FGF1, FGF2 and EGF gene polymorphisms and psoriatic arthritis, BMC Musculoskelet. Disord. 8 (2007) 1, https://doi.org/10.1186/1471-2474-8-1.

[17] Y. Zhao, J. Hu, X. Sun, K. Yang, L. Yang, L. Kong, B. Zhang, F. Li, C. Li, B. Shi, K. Hu, A. Sun, J. Ge, Loss of m6A demethylase ALKBH5 promotes post-ischemic angiogenesis via post-transcriptional stabilization of WNT5A, Clin. Transl. Med. 11 (2021) e402, https://doi.org/10.1002/ctm2.402.

[18] T.E. Ryan, D.J. Yamaguchi, C.A. Schmidt, T.N. Zeczycki, S.R. Shaikh, P. Brophy, T.D. Green, M.D. Tarpey, R. Karnekar, E.J. Goldberg, G.C. Sparagna, M. J. Torres, B.H. Annex, P.D. Neufer, E.E. Spangenburg, J.M. McClung, Extensive skeletal muscle cell mitochondriopathy distinguishes critical limb ischemia patients from claudicants, JCI Insight 3 (2018) e123235, https://doi.org/10.1172/jci.insight.123235.

[19] B. Alipanahi, A. Delong, M.T. Weirauch, B.J. Frey, Predicting the sequence specificities of DNA- and RNA-binding proteins by deep learning, Nat. Biotechnol. 33 (2015) 831–838, https://doi.org/10.1038/nbt.3300.

[20] W. Han, S. Wang, Y. Qi, F. Wu, N. Tian, B. Qiang, X. Peng, Targeting HOTAIRM1 ameliorates glioblastoma by disrupting mitochondrial oxidative phosphorylation and serine metabolism, iScience 25 (2022) 104823, https://doi.org/10.1016/j.isci.2022.104823.

[21] Y. Hu, Y. Zhao, N. Dai, H. Lu, J. Ge, Unwavering excellence: how to be a competent cardiovascular doctor in "panvascular medicine +," Innovation 4 (2023) 100489 https://doi.org/10.1016/j.xinn.2023.100489.

[22] M. Wong, Y. Dai, J. Ge, Pan-vascular disease: what we have done in the past and what we can do in the future? Cardiol. 9 (2024) 1–5, https://doi.org/10.1097/CP9.0000000000000078.

[23] Y. Hu, Y. Zhao, P. Li, H. Lu, H. Li, J. Ge, Hypoxia and panvascular diseases: exploring the role of hypoxia-inducible factors in vascular smooth muscle cells under panvascular pathologies, Sci. Bull. 68 (2023) 1954–1974, https://doi.org/10.1016/j.scib.2023.07.032.

[24] V. Aboyans, J.-B. Ricco, M.-L.E.L. Bartelink, M. Björck, M. Brodmann, T. Cohnert, J.-P. Collet, M. Czerny, M. De Carlo, S. Debus, C. Espinola-Klein, T. Kahan, S. Kownator, L. Mazzolai, A.R. Naylor, M. Roffi, J. Röther, M. Sprynger, M. Tendera, G. Tepe, M. Venermo, C. Vlachopoulos, I. Desormais, ESC Scientific Document Group, P. Widimsky, P. Kolh, S. Agewall, H. Bueno, A. Coca, G.J. De Borst, V. Delgado, F. Dick, C. Erol, M. Ferrini, S. Kakkos, H.A. Katus, J. Knuuti, J. Lindholt, H. Mattle, P. Pieniazek, M.F. Piepoli, D. Scheinert, H. Sievert, I. Simpson, J. Sulzenko, J. Tamargo, L. Tokgozoglu, A. Torbicki, N. Tsakountakis, J. Tuñón, M.V. De Ceniga, S. Windecker, J.L. Zamorano, S. Windecker, V. Aboyans, S. Agewall, E. Barbato, H. Bueno, A. Coca, J.-P. Collet, I. M. Coman, V. Dean, V. Delgado, D. Fitzsimons, O. Gaemperli, G. Hindricks, B. Iung, P. Juni, H.A. Katus, J. Knuuti, P. Lancellotti, C. Leclercq, T. McDonagh, M. F. Piepoli, P. Ponikowski, D.J. Richter, M. Roffi, E. Shlyakhto, I.A. Simpson, J.L. Zamorano, P.H. Zelveian, M. Haumer, D. Isachkin, T. De Backer, M. Dilic, I. Petrov, M.V. Kirhmajer, D. Karetova, E. Prescott, H. Soliman, A. Paapstel, K. Makinen, S. Tosev, E. Messas, Z. Pagava, O.J. Müller, K.K. Naka, Z. Járai, T. Gudjonsson, M. Jonas, S. Novo, P. Ibrahimi, O. Lunegova, V. Dzerve, N. Misonis, J. Beissel, E. Pllaha, M. Taberkant, T. Bakken, R. Teles, D. Lighezan, A. Konradi, M. Zavatta, J. Madaric, Z. Fras, L.S. Melchor, U. Näslund, B. Amann-Vesti, A. Obiekezie, ESC guidelines on the diagnosis and treatment of peripheral arterial diseases, in collaboration with the European society for vascular surgery (ESVS), Eur. Heart J. 39 (2018) (2017) 763–816, https://doi.org/10.1093/eurheartj/ehx095.

[25] T.W. Rooke, A.T. Hirsch, S. Misra, A.N. Sidawy, J.A. Beckman, L.K. Findeiss, J. Golzarian, H.L. Gornik, J.L. Halperin, M.R. Jaff, G.L. Moneta, J.W. Olin, J. C. Stanley, C.J. White, J.V. White, R.E. Zierler, ACCF/AHA focused update of the guideline for the management of patients with peripheral artery disease (updating the 2005 guideline), J. Am. Coll. Cardiol. 58 (2011) (2011) 2020–2045, https://doi.org/10.1016/j.jacc.2011.08.023.

[26] M.H. Criqui, V. Aboyans, Epidemiology of peripheral artery disease, Circ. Res. 116 (2015) 1509–1526, https://doi.org/10.1161/CIRCRESAHA.116.303849.

[27] S.X.Y. Soon, A. Patel, T.T. Chong, C.J.Q. Yap, H.T. Tay, K.H. Tay, C. Sivanathan, T.Y. Tang, Distribution of peripheral arterial disease in patients undergoing endovascular revascularization for chronic limb threatening ischaemia: insights from the vascular quality initiative in Singapore, Vasc. Spec. Int. 37 (2021) 13, https://doi.org/10.5758/vsi.210016.

[28] T. Alsaigh, B.A. Di Bartolo, J. Mulangala, G.A. Figtree, N.J. Leeper, Bench-to-Bedside in vascular medicine: optimizing the translational pipeline for patients with peripheral artery disease, Circ. Res. 128 (2021) 1927–1943, https://doi.org/10.1161/CIRCRESAHA.121.318265.

[29] Q.-Y. Du, Z.-M. Zhu, D.-S. Pei, The biological function of IGF2BPs and their role in tumorigenesis, Invest. N. Drugs 39 (2021) 1682–1693, https://doi.org/10.1007/s10637-021-01148-9.

[30] J. Cao, Q. Mu, H. Huang, The roles of insulin-like growth factor 2 mRNA-binding protein 2 in cancer and cancer stem cells, Stem Cell. Int. 2018 (2018) 1–15, https://doi.org/10.1155/2018/4217259.

[31] H. Ding, T. Wu, Insulin-like growth factor binding proteins in autoimmune diseases, Front. Endocrinol. 9 (2018) 499, https://doi.org/10.3389/fendo.2018.00499.

[32] K. Wächter, M. Köhn, N. Stöhr, S. Hüttelmaier, Subcellular localization and RNP formation of IGF2BPs (IGF2 mRNA-binding proteins) is modulated by distinct RNA-binding domains, Bchm 394 (2013) 1077–1090, https://doi.org/10.1515/hsz-2013-0111.

[33] H. Boughanem, E.M. Yubero-Serrano, J. López-Miranda, F.J. Tinahones, M. Macias-Gonzalez, Potential role of insulin growth-factor-binding protein 2 as therapeutic target for obesity-related insulin resistance, Int. J. Mol. Sci. 22 (2021) 1133, https://doi.org/10.3390/ijms22031133.

[34] H.-H. Wu, N.-J. Liu, Z. Yang, X.-M. Tao, Y.-P. Du, X.-C. Wang, B. Lu, Z.-Y. Zhang, R.-M. Hu, J. Wen, IGF2BP2 and obesity interaction analysis for type 2 diabetes mellitus in Chinese Han population, Eur. J. Med. Res. 19 (2014) 40, https://doi.org/10.1186/2047-783X-19-40.

[35] T. Jia, T. Jacquet, F. Dalonneau, P. Coudert, E. Vaganay, C. Exbrayat-Héritier, J. Vollaire, V. Josserand, F. Ruggiero, J.-L. Coll, B. Eymin, FGF-2 promotes angiogenesis through a SRSF1/SRSF3/SRPK1-dependent axis that controls VEGFR1 splicing in endothelial cells, BMC Biol. 19 (2021) 173, https://doi.org/10.1186/s12915-021-01103-3.

[36] Jiang L, Li Y, He Y, Wei D, Yan L, Wen H, Knockdown of m6A Reader IGF2BP3 Inhibited Hypoxia-Induced Cell Migration and Angiogenesis by Regulating Hypoxia Inducible Factor-1α in Stomach Cancer, Front Oncol (2021). Sep 21;11:711207. doi: 10.3389/fonc.2021.711207. PMID: 34621671; PMCID: PMC8490730.

[37] Yang Z, Wang T, Wu D, Min Z, Tan J, Yu B. RNA N6-methyladenosine reader IGF2BP3 regulates cell cycle and angiogenesis in colon cancer. J Exp Clin Cancer Res. 2020;39(1):203. Published 2020 Sep 29. doi:10.1186/s13046-020-01714-8.

[38] H. Fang, Q. Sun, J. Zhou, H. Zhang, Q. Song, H. Zhang, G. Yu, Y. Guo, C. Huang, Y. Mou, C. Jia, Y. Song, A. Liu, K. Song, C. Lu, R. Tian, S. Wei, D. Yang, Y. Chen, T. Li, K. Wang, Y. Yu, Y. Lv, K. Mo, P. Sun, X. Yu, X. Song, m6A methylation reader IGF2BP2 activates endothelial cells to promote angiogenesis and metastasis of lung adenocarcinoma, Mol. Cancer 22 (2023) 99, https://doi.org/10.1186/s12943-023-01791-1.

[39] Y. Bian, Y. Wang, S. Xu, Z. Gao, C. Li, Z. Fan, J. Ding, K. Wang, m6A modification of long non-coding RNA HNF1A-AS1 facilitates cell cycle progression in colorectal cancer via IGF2BP2-mediated CCND1 mRNA stabilization, Cells 11 (2022) 3008, https://doi.org/10.3390/cells11193008.

[40] I.A. Elcheva, C.P. Gowda, D. Bogush, S. Gornostaeva, A. Fakhardo, N. Sheth, K.M. Kokolus, A. Sharma, S. Dovat, Y. Uzun, T.D. Schell, V.S. Spiegelman, IGF2BP family of RNA-binding proteins regulate innate and adaptive immune responses in cancer cells and tumor microenvironment, Front. Immunol. 14 (2023) 1224516, https://doi.org/10.3389/fimmu.2023.1224516.

[41] H. Huang, H. Weng, W. Sun, X. Qin, H. Shi, H. Wu, B.S. Zhao, A. Mesquita, C. Liu, C.L. Yuan, Y.-C. Hu, S. Hüttelmaier, J.R. Skibbe, R. Su, X. Deng, L. Dong, M. Sun, C. Li, S. Nachtergaele, Y. Wang, C. Hu, K. Ferchen, K.D. Greis, X. Jiang, M. Wei, L. Qu, J.-L. Guan, C. He, J. Yang, J. Chen, Recognition of RNA N6-methyladenosine by IGF2BP proteins enhances mRNA stability and translation, Nat. Cell Biol. 20 (2018) 285–295, https://doi.org/10.1038/s41556-018-0045-z.
[42] Y. Nakamura, Multiple therapeutic applications of RBM-007, an anti-FGF2 aptamer, Cells 10 (2021) 1617, https://doi.org/10.3390/cells10071617.
[43] A. Sedlář, M. Trávníčková, R. Matějka, Š. Pražák, Z. Mészáros, P. Bojarová, L. Bačáková, V. Křen, K. Slámová, Growth factors VEGF-A165 and FGF-2 as multifunctional biomolecules governing cell adhesion and proliferation, Int. J. Mol. Sci. 22 (2021) 1843, https://doi.org/10.3390/ijms22041843.
[44] B. Gharibi, F.J. Hughes, Effects of medium supplements on proliferation, differentiation potential, and in vitro expansion of mesenchymal stem cells, Stem Cells Transl. Med. 1 (2012) 771–782, https://doi.org/10.5966/sctm.2010-0031.
[45] P.A. Underwood, J.M. Whitelock, P.A. Bean, J.G. Steele, Effects of base material, plasma proteins and FGF2 on endothelial cell adhesion and growth, J. Biomater. Sci. Polym. Ed. 13 (2002) 845–862, https://doi.org/10.1163/156856202320401924.
[46] Y.M. Shin, Y.B. Lee, S.J. Kim, J.K. Kang, J.-C. Park, W. Jang, H. Shin, Mussel-inspired immobilization of vascular endothelial growth factor (VEGF) for enhanced endothelialization of vascular grafts, Biomacromolecules 13 (2012) 2020–2028, https://doi.org/10.1021/bm300194b.
[47] Y.H. Shen, M.S. Shoichet, M. Radisic, Vascular endothelial growth factor immobilized in collagen scaffold promotes penetration and proliferation of endothelial cells, Acta Biomater. 4 (2008) 477–489, https://doi.org/10.1016/j.actbio.2007.12.011.
[48] D.E. Robinson, L.E. Smith, D.A. Steele, R.D. Short, J.D. Whittle, Development of a surface to enhance the effectiveness of fibroblast growth factor 2 (FGF-2), Biomater. Sci. 2 (2014) 875–882, https://doi.org/10.1039/c4bm00018h.
[49] N. Firoozi, Y. Kang, Immobilization of FGF on poly(xylitol dodecanedioic acid) polymer for tissue regeneration, Sci. Rep. 10 (2020) 10419, https://doi.org/10.1038/s41598-020-67261-6.
[50] T. J, R. Z, B. E, M. P, R. T, Endothelialization of an ePTFE vessel prosthesis modified with an antithrombogenic fibrin/heparin coating enriched with bound growth factors, RSC Adv. 11 (2021), https://doi.org/10.1039/d1ra00053e.